Automatic Measurement of Pearlite Spacing by Spectral Analysis

AUTOMATIC MEASUREMENT OF PEARLITE SPACING BY SPECTRAL ANALYSIS

Paolo Matteis

Politecnico di Torino, DISAT, Torino, Italy

Published in *Metallography, Microstructure and Analysis* on March, 16, 2020.

DOI: 10.1007/s13632-020-00630-9

ABSTRACT: The properties of pearlitic steels are determined mainly by the pearlite interlamellar spacing. This parameter can be readily measured on a micrograph of a polished and etched cross section, by using manual counting methods, but the automatic measurement of the same parameter is still challenging. A spectral method to measure the pearlite spacing, based on the bi-dimensional discrete Fourier transform, is here proposed and described in detail. The results obtained with this method are generally consistent with those obtained by manual counting.

KEYWORDS: rail steel, pearlite spacing, automatic image analysis

1. Introduction

Pearlitic steels are widely used for the production of rails, as well as in other applications. The mechanical properties of such steels are determined mainly by the pearlite interlamellar spacing, which is the mean distance between successive cementite (or ferrite) lamellae within a pearlite colony. In turn, the pearlite spacing is determined by the final cooling or heat treatment. [1].

The pearlite spacing can be measured on a micrograph of a polished and etched cross section, with the appropriate stereological correction [2,3], and suitable polished specimens are often readily available because they are used for other routine quality controls, such as the oxide cleanness and surface decarburization analyses required by current rail standards [4].

Therefore, the measurement of interlamellar spacing could be a useful tool for quality control and evaluation of rails, as well as other pearlitic steel products.

Nevertheless, such measurement is not yet commonly used for quality control, because of the following limitations. In the first place, the interlamellar spacing of most contemporary pearlitic steel products is smaller than the resolution of the optical microscope, thus requiring the use of the scanning electron microscope (SEM), which in most industrial laboratories is available for advanced testing but not yet for routine work. In the second place, the measurement depends on human judgment and for this reason it is subjective and expensive.

Now the first limitation is being overcome by the increasing availability of desktop electron microscopes with low cost and adequate resolution. Therefore, the development of a fully automatic and repeatable procedure to determine the mean interlamellar spacing from a digital micrograph is addressed here.

2. Prior work

The true interlamellar spacing (S_t) of pearlite is the distance between the mid-planes of two successive cementite (or ferrite) lamellae in the same colony, measured in the direction perpendicular to the same lamellae. The true interlamellar spacing generally exhibits a significant variability among different pearlite colonies within the same steel sample [2], therefore in most cases it is necessary to calculate a mean value over several colonies. Unfortunately, the true spacing cannot be directly measured on a metallographic cross-section, because the angle between the lamellae and the cross-section plane is unknown; therefore, it is usually deduced either from the apparent spacing, or from the random spacing.

The apparent (S_a) and random (S_r) spacing are also the distance between successive lamellae, but the former is measured in the direction perpendicular to the traces of the lamellae on the observed cross-section, whereas the latter is measured in a random direction. The mean apparent spacing can be measured by counting the number of lamellae that intersect a line of known length, drawn on a micrograph, within a colony, and normal to the traces of the lamellae, then repeating over several colonies and averaging. In contrast, the mean random spacing can be measured by counting the number of lamellae that intersect a set of lines or circles of known total length, drawn at random on one or more micrographs, over either one colony or several adjacent colonies. [2,3]

The mean true pearlite spacing, $\bar{S}_t$, can then be derived from the mean apparent or random spacing by taking into account the random spatial distribution of the pearlite colonies, with the stereological correlations [3]:

$$\bar{S}_t = (\pi/4) \cdot \bar{S}_a = (1/2) \cdot \bar{S}_r$$

The above methods can be employed by a skilled human operator, but are difficult to automate, even if several attempts were made in this direction.

Petitgand et al. [2] compared several methods based on image segmentation, whereby the original grayscale micrograph is first reduced into a binary picture (in which for example cementite is white and ferrite is black) and then examined by using morphological methods. However, all these methods require sharp images of single colonies at very high magnification, between 100 000x and 200 000x, meaning that they are still beyond the capabilities of low-cost desktop SEMs (even if a much lower magnification is sufficient for human visual examination), and also require expert human judgment in the choice of the field of view and magnification.

The same authors also mentioned the possible use of spectral methods, based on the Fourier transform rather than on image segmentation, but they did not develop a fully automated procedure,

leaving to the human operator the task of identifying and interpreting the significant spots in the Fourier transform [2].

Spectral analysis was also previously proposed for other image analysis tasks related to steel metallography, including the assessment of banding [5] and of grain orientation due to plastic deformation [6], and is here employed in the development of a fully automated method for the measurement of the pearlite spacing.

3. Spectral analysis concept

The image of one pearlite colony on a polished and etched cross section can be described as a periodic pattern, whose wavelength is the apparent interlamellar spacing; and the image of several adjacent colonies on the same cross section can also be described as a set of adjacent periodic patterns, whose mean wavelength is the mean apparent interlamellar spacing. Therefore, the apparent pearlite spacing can be determined by analyzing the micrograph in the frequency (or wavenumber) domain, i.e., by using spectral analysis.

This can be accomplished by using a centered bi-dimensional Discrete Fourier Transform (DFT), a well known mathematical tool which allows to decompose a picture into a sum of periodic components, with no loss of information.

A monochrome digital micrograph and its DFT are both bi-dimensional arrays of numbers, of the same size. Each element, or pixel, of the original micrograph is a real number and represents the brightness of a point of given horizontal and vertical coordinates on the specimen surface; in contrast, each element of the corresponding DFT is a complex number and represents the magnitude and phase of a sinusoidal function of given horizontal and vertical wavelength, the sum of all such functions being equal to the original micrograph.

The bi-dimensional DFT can be readily calculated by using numerical algorithms, which are implemented in several widespread software packages; computationally efficient DFT algorithms are also know as Fast Fourier Transform, or FFT, algorithms.

If the micrograph exhibits periodic patterns, such as the pearlite colonies, the magnitude of its DFT exhibits sharp local maxima corresponding to the dominant wavenumbers (or inverse wavelengths) of such patterns. In particular, pearlite colonies exhibiting vertical, oblique or horizontal lamellae with the same spacing will contribute to different local maxima of the magnitude of DFT.

Since for the present purpose the orientation (vertical, oblique or horizontal) of the pearlite lamellae is irrelevant, in this work the DFT is divided into sets of elements, each corresponding (approximately) to the same pearlite spacing (or total wavenumber) and encompassing all possible orientations. Then the total magnitude of each set is plotted against its wavenumber. Such plot usually exhibits a sharp peak. Finally, the position of such peak in the spectral plot is interpreted as the dominant wavenumber of the examined micrograph.

If the micrograph exhibits only one colony, its dominant wavenumber is the inverse of its wavelength, which is the apparent pearlite spacing of the examined colony. If, in contrast, the

micrograph exhibits several colonies, it is assumed that the dominant wavenumber corresponds to the mean apparent spacing.

4. Implementation and examples

The bi-dimensional DFT, $\boldsymbol{F}$, of the digital micrograph $\boldsymbol{I}$ of size M, N is:

$$F_{u,v} = \sum_{p=0}^{M-1} \sum_{q=0}^{N-1} I_{m,n} \cdot exp\left[-2\pi i \left(\frac{u \cdot p}{M} + \frac{v \cdot q}{N}\right)\right]$$

where i is the imaginary unit. The DFT is periodic with period M, N (in other words, if both α and β are integers, it follows that $F_{u,v} = F_{u+\alpha \cdot M, v+\beta \cdot N}$); therefore $\boldsymbol{F}$ has $M \cdot N$ independent elements.

Ordinarily, the DFT is calculated for $u = 0, \dots, M-1$ and $v = 0, \dots, N-1$. However, for the purpose of image analysis, it is more convenient to calculate $\boldsymbol{F}$ for $u = -\lfloor M/2 \rfloor, \dots, \lceil M/2 \rceil - 1$ and $v = -\lfloor N/2 \rfloor, \dots, \lceil N/2 \rceil - 1$. The latter choice is called the centered DFT and, thanks to the abovementioned periodicity, it is readily obtained from the ordinary DFT by circularly shifting its rows and columns by $\lfloor M/2 \rfloor$ and $\lfloor N/2 \rfloor$ steps, respectively.

An example of the above calculation is given in figure 1, where the cross-section micrograph of two pearlite colonies at high magnification (figure 1a) and of several adjacent pearlite colonies at comparatively lower magnification (figure 1b) are shown alongside the magnitude of their respective centered DFTs (figures 1c and 1d). Both micrographs in this example have been obtained from the same specimen, by means of scanning electron microscopy, with different magnification; the resolution is 10.5 and 52.5 nm/px, respectively, for figure 1a and 1b.

Different elements of $\boldsymbol{F}$ can encompass several orders of magnitude; moreover, $F_{0,0}$ is the sum of all elements of $\boldsymbol{I}$ and is usually much greater than all other elements of $\boldsymbol{F}$ (because pictures are represented by using positive numbers only).

For these reasons, and to improve readability, figures 1c and 1d are plotted by using a logarithmic grayscale, where black and white represent the minimum and second-maximum values, respectively. Therefore, the pixel corresponding to $F_{0,0}$ is saturated and appears as a white point in the center.

Since $\boldsymbol{I}$ is real, $F_{u,v}$ is the complex conjugate of $F_{-u,-v}$ and they have the same magnitude; for this reason, figures 1b and 1d, as well as any other picture made with the above procedure, exhibit central symmetry.

Since figure 1a exhibits two periodic features (i.e., two pearlite colonies), the magnitude of its DFT in figure 1c exhibits two pairs of bright spots (other than the above mentioned central point), which are each related to one of them; bright spots come in pairs due to the central symmetry. In contrast, since figure 1b exhibits several periodic colonies, the magnitude of its DFT in figure 1d exhibits an halo formed by several less intense spots.

$F_{u,v}$ is a complex number and its magnitude represents the amplitude of the sinusoidal component of $\boldsymbol{I}$ having vertical and horizontal wavenumbers equal to u/M and v/N, respectively, and total wavenumber equal to:

$$W_{u,v} = \sqrt{(u/M)^2 + (v/N)^2}$$

where the unit of measure of the wavenumbers is the inverse of one pixel, or px^{-1} (with reference to the original micrograph $\boldsymbol{I}$). Therefore, in the u,v Cartesian plane, the locus of the points which correspond to the same total wavenumber W is an ellipse (or a circle if $M = N$), and a greater wavenumber corresponds to a greater ellipse (or circle).

Since only the total wavenumber is relevant (and not its horizontal and vertical components), in this work $\boldsymbol{F}$ is split into several subsets, each consisting of elements having approximately the same total wavenumber, and therefore lying close to the same ellipse in the u,v Cartesian plane. This is accomplished as follows.

First, for each couple of array indexes u,v, a corresponding linear index n is calculated as:

$$n(u,v) = \left\lfloor W_{u,v} \cdot \sqrt{M \cdot N} + 0.5 \right\rfloor$$

Since n is proportional to the wavenumber $W_{u,v}$, all elements $F_{u,v}$ that have the same linear index n also correspond approximately to the same wavenumber $W_n = n/\sqrt{M \cdot N}$.

Then, for each value of n, other than zero, the total spectral magnitude F_n is calculated as the sum of the magnitude of all elements $F_{u,v}$ having the index n. The case $u = v = n = 0$ is not considered because $F_{0,0}$ represents the non-periodic component of $\boldsymbol{I}$, which is irrelevant for the present purposes.

In the above steps, the coefficient $\sqrt{M \cdot N}$ is arbitrary and it is chosen in order to obtain approximately the same spectral resolution in the vector F_n as in the array $\boldsymbol{F}$.

Finally, the total spectral magnitude F_n can be plotted against the corresponding wavenumber W_n.

Unfortunately, $\boldsymbol{F}$ usually exhibits a positive background noise, which could influence the above result. In fact, the contribution of the background noise to F_i is proportional to the number of elements of $\boldsymbol{F}$ that must be added together to get F_i, which in turn is proportional to i and hence to W_i (W_i and F_i being the i-th elements of W_n and F_n), at least up to about $W_i = 0.5$.

To correct this effect, a constant background noise value B is subtracted from $\boldsymbol{F}$ before calculating F_n. For this purpose, first the histogram of $\boldsymbol{F}$ is calculated, excluding the greater 0.1% of elements; then B is assumed equal to the position of the peak of the histogram. The peak position is determined by Gaussian fitting of the relevant portion of the histogram; the fitting domain is adjusted iteratively and eventually corresponds to the full width at half maximum of the Gaussian peak.

The plot of the total spectral magnitude F_n against the corresponding wavenumber W_n, as obtained with the above steps, for the same micrographs that are shown in figure 1, is here reported in figure 2. The total spectral magnitude is expressed in arbitrary units, because it derives from the arbitrary scaling of the grey levels in the original micrograph.

In both cases in figure 2, the spectral plot exhibits a sharp maximum, which roughly corresponds to the total wavenumber of the bright spots in figures 2b and 2d. In particular, figure 2a exhibits a narrow peak that derives in large part from a single pearlite colony, with a small contribution from another one (figure 1b), whereas figure 2b exhibits a broader peak that derives from several different colonies (figure 1d). In the latter case, the greater peak width likely depends on the variability of the apparent interlamellar spacing among the different colonies that are examined together.

The wavenumber corresponding to the position of the above mentioned peak in the spectral plot is here interpreted as the dominant wavenumber of the original micrograph. This wavenumber is determined by Gaussian fitting of the relevant portion of the same plot (also in this case, the fitting domain is adjusted iteratively and eventually corresponds to the full width at half maximum of the Gaussian peak). Finally, the apparent pearlite spacing is calculated as the inverse of the dominant wavenumber.

For example, the dominant wavenumber for figures 1a and 1b, calculated with the above procedure, is 0.0382 and 0.1975 px^{-1}, and the corresponding pearlite spacing is 26.2 and 5.06 px, respectively. By taking into account the above mentioned resolution of the two micrographs, the calculated apparent pearlite spacing is 276 and 267 nm, respectively.

As a further verification, the dominant wavenumber can also be calculated as the weighted mean wavenumber of the region of $\boldsymbol{F}$ which contains the abovementioned continuous halo or discrete bright spots, by using the magnitude of $\boldsymbol{F}$ as the weight of each point. This calculation was performed here by considering all points of $W_{u,v}$ that fall within the full width at half maximum of the peak of the spectral plot, weighted by using the magnitude of the corresponding points of $F_{u,v}$. The result is almost exactly the same as the above calculation.

5. Testing

The above described spectral measurement method was tested on two rail steel batches. The steels elemental composition, as shown in Table 1, was determined by Atomic Emission Spectroscopy with spark excitation (spark-AES) and is compliant to the R260 European rail steel grade [4].

For each steel, one metallographic specimen was cut from a finished rail, in the standard rail head position for microstructure control prescribed by current norms for rail steel [4]. The specimens were then mounted, polished, etched with 3% Nital (97 % ethanol - 3% nitric acid) and examined.

The microstructure of both steels was found to be nearly fully pearlitic (with rare traces of ferrite on the prior austenitic grain boundaries), as shown in Fig. 1a and 1b here above.

Finally, the micrographs for the measurement of the apparent pearlite spacing were obtained by SEM, with the same image size of 1024 x 884 pixels and grey resolution of 256 levels, and with nominal magnification values in the 2000x to 25000x range, corresponding to actual resolution in the 10.5 to 132 nm/px range.

The apparent pearlite spacing was then measured on the same micrographs by using either a manual measurement method or the above described spectral algorithm.

The following manual counting measurement method was used. Ten intended measurement points were chosen at random in each micrograph; whenever possible (i.e., whenever the pearlite lamellae around the intended measurement point were clearly resolved), a measurement line perpendicular to the pearlite lamellae was drawn through each measurement point and extended in both directions up to either the pearlite colony boundary or the picture edge; the apparent pearlite spacing of each measurement point was determined as the ratio of the length of its measurement line over the number of cementite lamellae intersected by the same line; and finally the apparent pearlite spacing of each micrograph was determined as the mean of the apparent pearlite spacing values of its measurement points. The standard deviation of all measurements performed on the same micrograph was also calculated. The details of these measurements are reported in table II.

The spectral algorithm was implemented by using the Matlab programming code (available from The MathWorks Inc., Natick, Massachusetts, USA) and it is attached to this paper as supplementary material.

The resulting code is fully automatic and runs in less than 1.5 second per picture on a desktop pc (even if it was not optimized for speed). The micrographs employed in these calculations, their DFTs, and their ensuing spectral plots are also here attached as supplementary material.

6. Results and discussion

The results of both automatic and manual measurements are shown and compared in table III.

The difference between the two methods is less than 15 % in all cases but one, and the value obtained from the automatic measurement falls within the uncertainty band of the manual measurement (defined as the mean plus or minus one standard deviation) in all cases but one.

The apparent spacing values measured on the pearlite micrographs by using the automatic spectral procedure are on average 10% greater than those obtained by the manual counting method. This small bias seems to arise both for micrographs showing only one colony and for those showing several colonies. For comparison, tests performed on artificial images showing a single set of alternate parallel black and white strips, with constant spatial frequency and added random noise, returned nearly exactly the same values with the two measurement methods. Therefore, it is here hypothesized that the above noted difference arises from how the two methods take account of the imperfections in the shape of the cementite lamellae, in respect to the ideal model, e.g. the fact that the cementite lamellae within one colony are not perfectly parallel and equidistant, and may start and end within the colony and not only on its boundary.

Measurement performed on the same steel batch are also in most cases quite close between them, even if the magnification and field of view are different, with the exception of micrograph 1 of steel A, which returned a significantly higher apparent spacing.

Micrograph 1 of steel A is also the micrograph with the lowest nominal magnification (2000 x), and in which more manual measurements points are missing (because they fall within unresolved areas);

therefore, in this case probably both the manual and the automatic analysis procedures are similarly biased because only the pearlite colonies showing the larger apparent spacing are resolved.

The maximum wavenumber represented by at least one point in the DFT is about 0.7 px^{-1}, but the number of points representing wavenumbers greater 0.5 px^{-1} falls sharply by increasing the wavenumber; therefore the theoretical minimum spacing that could be measured, by using the spectral method, is about 2 px. In contrast, the apparent pearlite spacing of micrograph 1 of steel A is about 4.2 pixel. Therefore, the minimum magnification is not determined solely by the minimum measurable apparent spacing, but rather it must be increased to take into account the variability of the apparent spacing between colonies.

For the here examined rail steels, nominal magnification of about 5000x or more, corresponding to actual resolution of about 50 nm/px or less, and leading to apparent mean pearlite spacing values greater than about 5 px, were found to be adequate.

Even if the resolution were adequate in all cases, a significant scatter should be expected among different micrographs recorded on the same sample. If the field of view were smaller than the mean size of the pearlite colonies, the scatter would reflect both the intrinsic variability of the true interlamellar spacing, and the random variation of the angle between the lamellae and the metallographic plane. Therefore, several micrographs should be used to calculate a reliable mean value. In contrast, if the field of view were larger, each measurement would be itself an average of several colonies, and less micrographs could be used, but the acquisition and calculation time for each micrograph would be greater (because a larger field of view with the same resolution implies larger pictures).

For the above reasons, for industrial applications, the resolution, the field of view and the number of micrographs should be standardized, on the basis of the desired accuracy.

Only the apparent interlamellar spacing has been calculated here, because it corresponds directly to the spatial periodicity shown by the pearlite colony on the observed cross-section; however, a reliable estimate of the random or true interlamellar spacing, if needed, can be readily obtained by using the well known stereological formulas that are reported here above in section 2.

The here proposed method could also be applied to determine the interlamellar spacing of the pearlite contained in a ferritic-pearlitic steel, or in other mixed-microstructure steels, if the examined pictures were so chosen as to exhibit either prevalently pearlitic areas, or single pearlite colonies.

7. Conclusions

A new method for automatic measurement of the apparent interlamellar spacing of pearlite by means of spectral analysis have been proposed and tested on fully pearlitic rail steels.

The results allow to conclude that the proposed method is effective for micrographs showing either one or several colonies, as long as the apparent pearlite spacing at the employed magnification is at least 5 pixel. For most rail steels this condition can be met by using low-cost desktop scanning

electron microscope, thus allowing in principle to use the automatic spectral measurement of the pearlite spacing as a routine quality control

References

[1] Krauss, G. (2015), *Steels: processing, structure, and performance*. ASM International, Materials Park, Ohio, USA, 315-321.

[2] Petitgand, H., Benoit, D., Moukassi, M., Debyser, B. Automatic measurement of pearlitic interlamellar spacing with computer image processing. *ISIJ International*, 1990, 30(7), 546-551.

[3] Vander Voort, G. F., Roosz, A. Measurement of the interlamellar spacing of pearlite. *Metallography*, 1984, 17(1), 1-17.

[4] EN 13674-1. Railway applications. Track. Rail. Vignole railway rails 46 kg/m and above. European Committee for Standardization, Brussels, Belgium, 2011

[5] From, A., Sandstrom, R.. Assessment of banding in steels by using advanced image analysis. *Materials characterization*, 1998, 41(1), 11-26.

[6] Holota, R., Nemecek, S. Recognition of oriented structures by 2D Fourier transform. In Pinker J. (ed.): *Applied Electronics*, 2002, University of West Bohemia, Pilsen 2002, pp. 88–92.

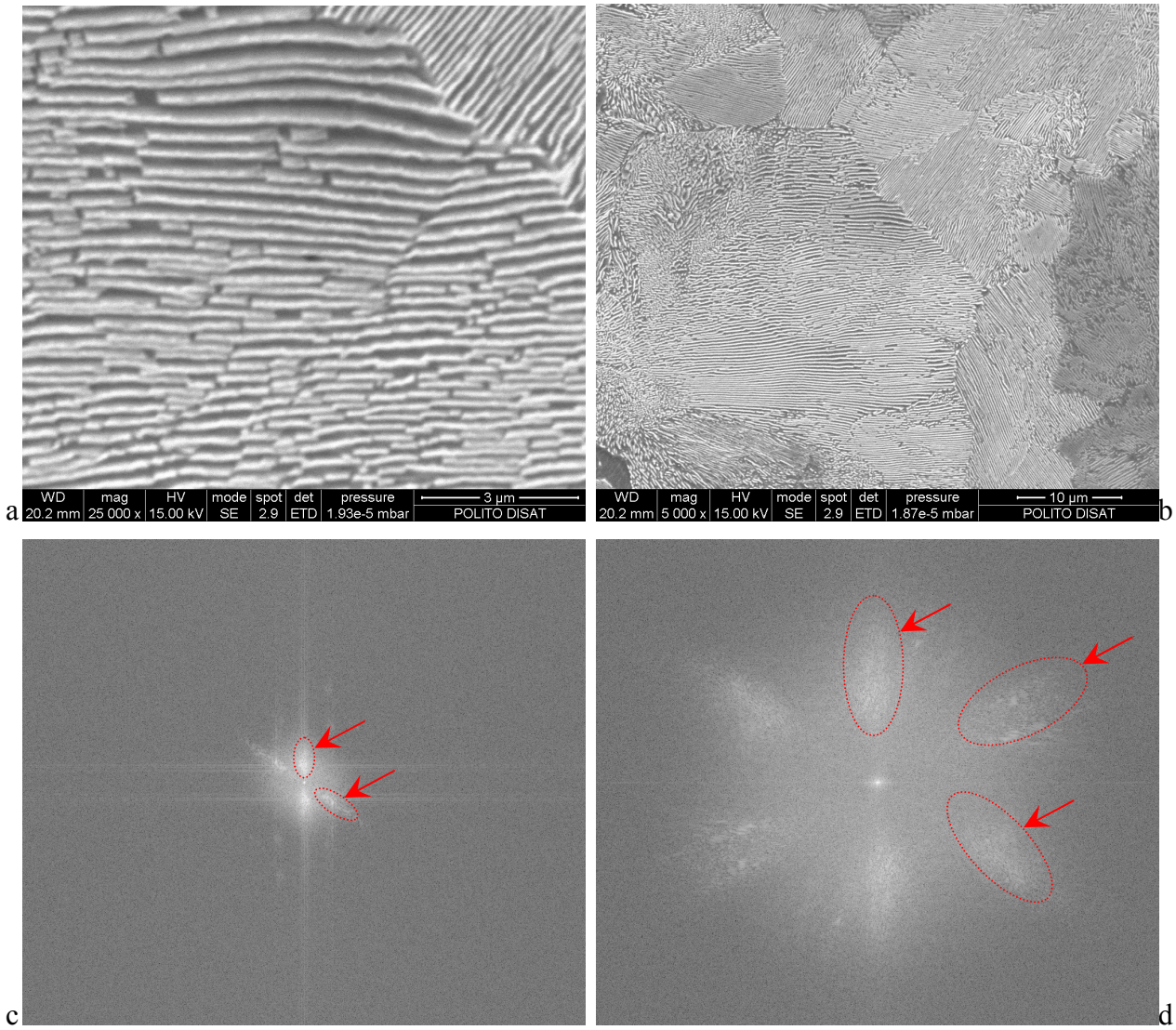

Fig 1 - Pearlite in a rail steel as observed by SEM, after Nital etching: micrographs with nominal magnification 25000x (a) and 5000x (b), and magnitude of their respective DFTs, plotted with a logarithmic scale (c and d). The arrows in c and d highlight some of the bright spots which are discussed in the text.

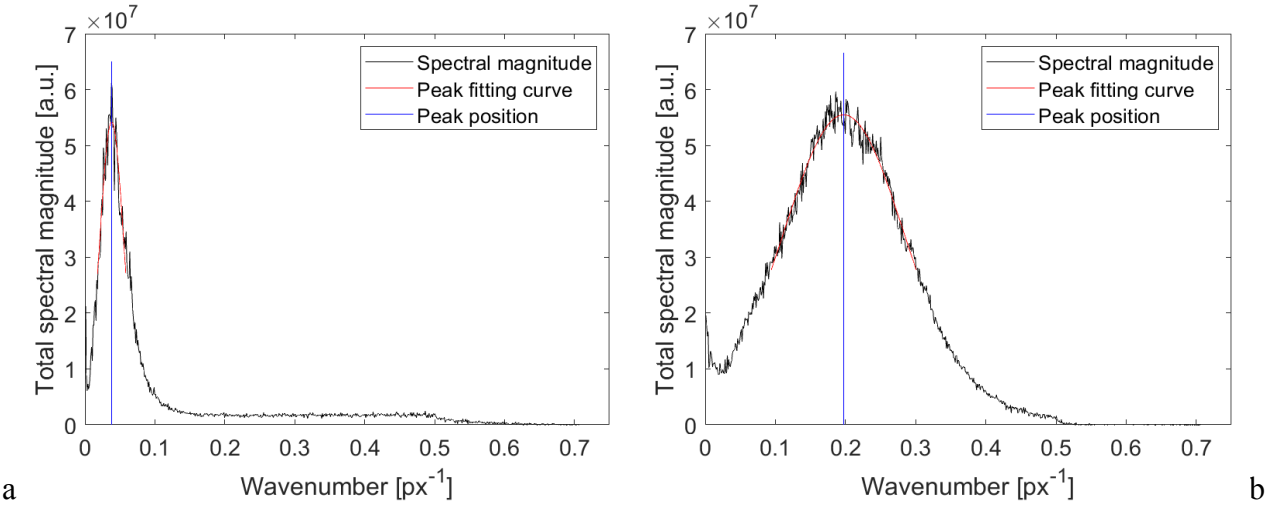

Fig. 2 - Spectral plots obtained from the DFTs represented in figures 1c and 1d (a and b, respectively).

Tab. I - Elemental composition of the examined rail steels (wt.%, bal. Fe), as obtained by spark-AES.

Rail steel	C	Si	Mn	P	S	Cr	Al	V	N
A	0.73	0.29	1.1	0.019	0.014	0.041	<0.001	0.001	0.0065
B	0.66	0.28	1.1	0.014	0.016	0.043	0.001	0.001	0.0064

Tab. II - Manual measurement of the apparent pearlite spacing. Steel heat (A or B); micrograph number (#), nominal magnification (Mag.) and resolution (Res.); mean apparent pearlite spacing ($\bar{S}_a$) in nanometers (nm); and mean value, standard deviation (st.dev.) and pointwise measured values of the apparent spacing in pixels (px). Some of the random intended measurement points fell within unresolved areas where measurement was not possible (n.m.).

Steel	#	Mag. [-]	Res. [nm/px]	$\bar{S}_a$ [nm]	Apparent spacing [px]										
					mean	st.dev.	1	2	3	4	5	6	7	8	9	10
A	1	2000	132	561	4.27	1.19	6.00	3.78	3.95	n.m.	n.m.	3.33	n.m.	n.m.	n.m.	n.m.
	2	4000	65.8	341	5.19	0.40	5.28	5.20	4.40	n.m.	n.m.	5.40	5.65	5.38	n.m.	5.00
	3	8000	32.9	341	10.37	4.40	9.75	6.64	6.44	20.89	12.00	6.74	9.50	9.10	13.95	8.65
	4	16000	16.4	265	16.10	5.58	15.83	20.25	13.28	13.61	13.64	13.80	14.74	12.86	12.34	30.63
B	1	5000	52.6	236	4.49	0.78	4.00	5.86	5.33	5.22	3.61	4.11	4.26	4.06	3.94	n.m.
	2	5000	52.6	299	5.68	1.05	5.67	4.22	6.85	5.71	5.91	4.26	4.53	6.03	7.14	6.53
	3	25000	10.5	273	25.94	1.44	27.09	26.82	26.24	26.66	23.11	23.46	26.18	26.19	26.48	27.13
	4	25000	10.5	248	23.56	5.25	20.42	18.00	17.71	30.43	29.31	25.47	23.38	20.22	19.35	31.31

Tab. III - Comparison of automatic and manual measurement of the apparent pearlite spacing. Steel heat (A or B); micrograph number (#), nominal magnification (Mag.) and resolution (Res.); manual and automatic (spectral) measurements of the apparent pearlite spacing in nanometers (nm) or pixels (px); and standard deviation (st.dev.) of manual measurements.

Heat	#	Mag. [-]	Res. [nm/px]	Manual analysis				Spectral analysis		Difference (spectral / manual)
				Spacing [nm]		Spacing [px]		Spacing [nm]	Spacing [px]	
				mean	st.dev.	mean	st.dev.			
A	1	2000	132	561	156	4.27	1.19	555	4.22	-1%
	2	4000	65.8	341	26	5.19	0.40	394	5.99	15%
	3	8000	32.9	341	145	10.37	4.40	358	10.9	5%
	4	16000	16.4	265	92	16.10	5.58	342	20.8	29%
B	1	5000	52.6	236	41	4.49	0.78	267	5.06	13%
	2	5000	52.6	299	55	5.68	1.05	324	6.16	8%
	3	25000	10.5	273	15	25.94	1.44	276	26.2	1%
	4	25000	10.5	248	55	23.56	5.25	276	26.2	11%